

Electronic Supplementary Information for “Artery-on-a-chip platform for automated, multimodal assessment of cerebral blood vessel structure and function”

Sanjesh Yasotharan, Sascha Pinto, John G. Sled, Steffen-Sebastian Bolz, and Axel Günther

Supplementary section S1 provides detail on the design of the artery-on-a-chip microfluidic device. Section S2 discusses the manifold design as well as the reversible seal between the manifold and the microfluidic device. Section S3 characterizes performance of on chip valves. Section S4 discusses the control of the artery temperature. Section S5 provides the boundary conditions and mesh resolution of the numerical simulation that is used to estimate the abluminal wall shear stress experienced by the smooth muscle cells (SMCs). Section S6 summarizes the custom LabView programs employed in the automated operation of the artery-on-a-chip platform. Section S7 lists the detailed staining protocols used for the data presented in the Section 3 of the paper.

S1. Artery-on-a-Chip Device Design and Fabrication

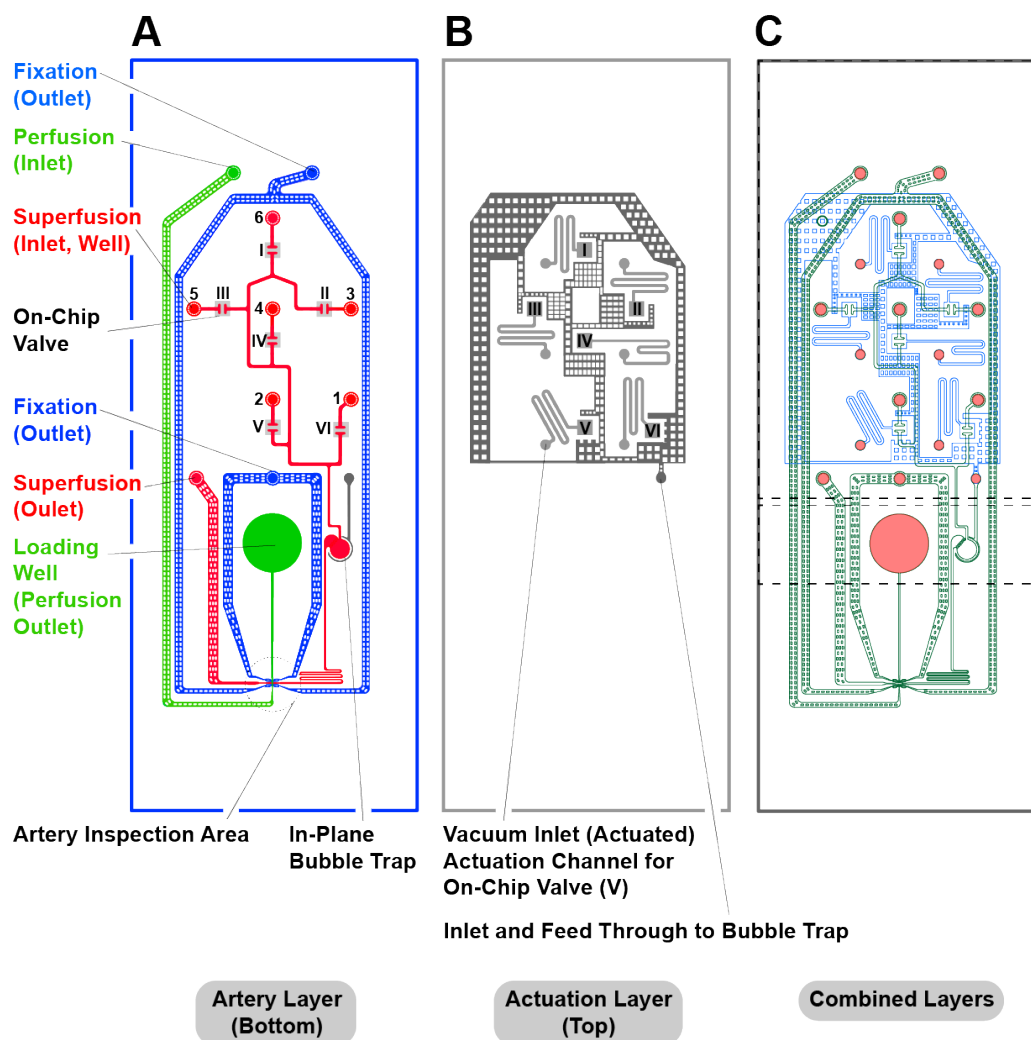
All devices consisted of three PDMS layers that were fabricated in poly(dimethylsiloxane) (PDMS) using standard multilayer soft lithography techniques involving three SU-8 masters. Figure S1.1A shows the footprints of the (center) artery layer and Fig. S1.1B shows the (top) actuation layer. The two layers were bonded to each other using a partial curing technique and attached to a bottom layer that contained a microscope slide (75 mm × 25 mm × 1mm).

We here briefly describe the complete fabrication sequence for the entire device from the bottom up. The sequence is schematically illustrated in Fig. S1.2A. Fabrication of the bottom layer (not shown in Fig. S1.1) starts from a commercially obtained glass slide (75 mm × 25 mm × 1mm, TA134, EMF, Ithaca, NY, USA) that is covered with a 100 nm gold coating on

top of a 5 nm titanium adhesion layer. Thin film resistance thermometers for recording the temperature in the proximity of a fixated artery segment were obtained by lithographically patterning positive resist (S1818, Shipley, Marlborough, MA, USA) and subsequent etching (TFTN, for titanium, Transcene, MA, USA). A thin layer of PDMS was spun onto the glass slide at 2000 rpm and cured to provide a consistent plasma bond (Harrick Plasma, Ithaca, NY, USA) during subsequent bonding steps. A <1mm thickness PDMS layer was cast onto a SU-8 master that defined the pillar array to be located underneath the inspection area. Unwanted bonding at the membrane locations of the on-chip valves was avoided by local deposition of a thermally curable fluoropolymer, CYTOP (Asahi Chemical Company, Japan), in areas below the PDMS membranes under a stereomicroscope.

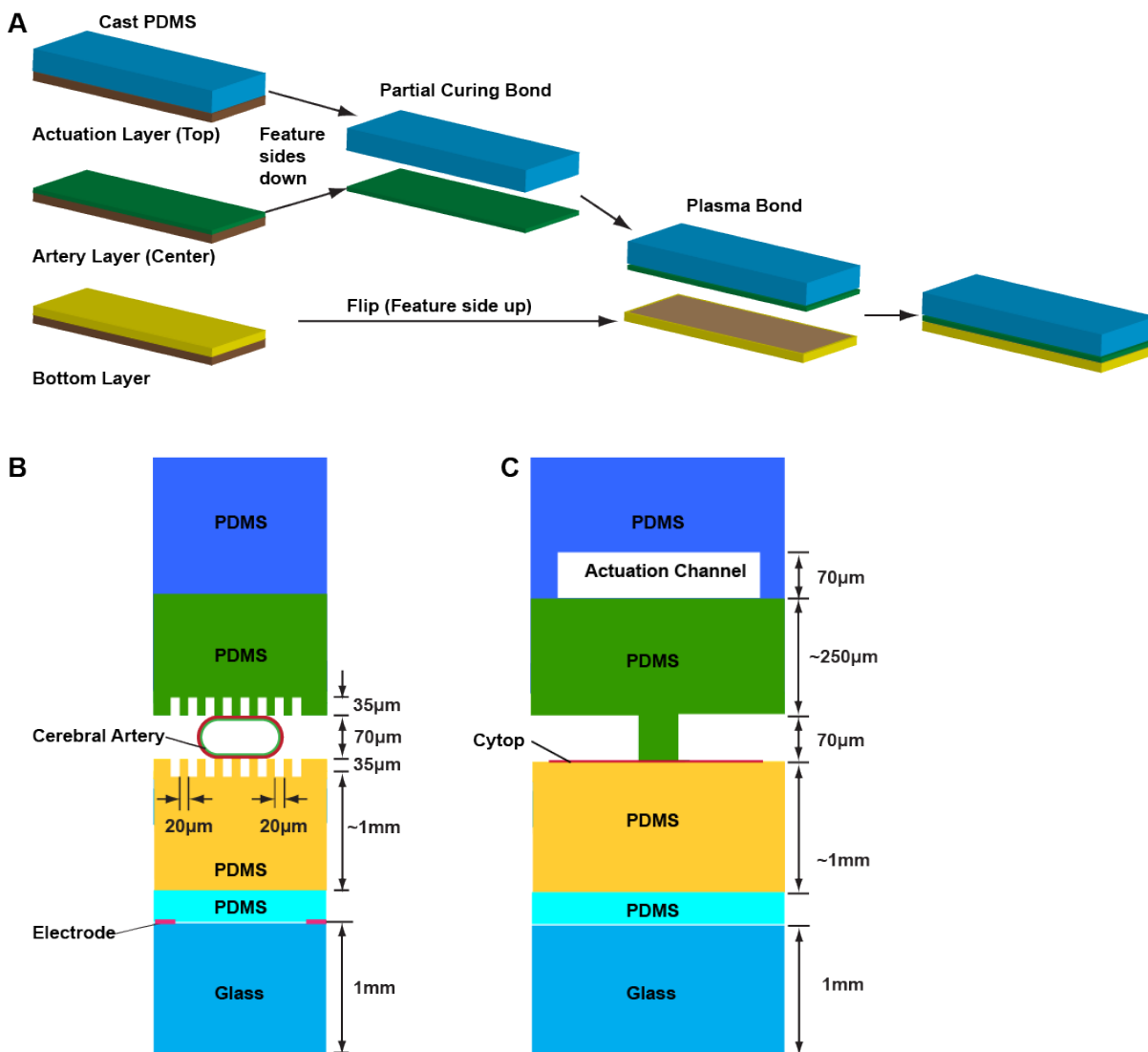
The (center) Artery Layer is shown in Fig. S1.1A. A dedicated SU-8 master defined the three liquid-carrying microchannel networks in direct contact with the artery segment, i.e., the perfusion channel network (green), the superfusion channel network (red) and the microchannel network for blood vessel immobilization (blue channels). The master had a uniform feature height of 70 μ m, except for the inspection area, where additional features were patterned with a second mask to locally define an array of 35 μ m tall micropillars. Spin coating PDMS onto the master at 400rpm defined the thin membrane (thickness \sim 300 μ m) used for actuating the on-chip valves. We refer to ESI Section S4 for more detail on the operation of the on chip valves. The (top) Actuation Layer is shown in Fig. S1.1B and accommodated the valve actuation channels. The layer was moulded from a SU-8 master with a uniform feature height of 70 μ m, peeled off and subsequently bonded to the Artery Layer via a previously reported partial curing technique.¹ After the combined PDMS layers were cured and peeled from the first master, they defined the top part of the device.

All valve actuation channels located in the top feature layer were initially primed with liquid by submerging the completed device in deionized water and degassing at a vacuum level of 20 inches of mercury for 2 hours. The device was subsequently stored in a vial of de-ionized water until use. The approach consistently prevented the unwanted nucleation and growth of gas bubbles during the hour-long periods of continuous operation.



FigureS1.1 Artery-on-a-Chip microfluidic device. (A) Channel footprint of Artery Layer (Center) accommodating networks of perfusion (green color), superfusion (red color), and fixation channels (blue). Superfusion solutions were delivered from six wells on manifold with individual on-chip valves (I-VI) for actuation. (B) Water-filled actuation layer containing actuation channels for on-chip valves (I-VI) as well as vacuum channels to prevent bubble generation. (C) Overlay of two layers with 17 fluidic inlet/outlet connections to manifold body shown in red color. Loading well shown in red color and position of

corresponding lid indicated with dashed line. Note that Bottom Layer containing thin-film resistance thermometers and pillar array below artery inspection area omitted.



FigureS1.2 (A) Artery-on-a-chip device fabrication sequence. (B) Schematic illustration of microfluidic device cross-sectional view at blood vessel location. (C) Schematic illustration of microfluidic device cross-sectional view at location of on chip valve.

S2. Manifold

A manifold was designed, milled in aluminum, anodized and tested. The manifold is shown in Fig. S2.1 and consisted of a manifold body, a base plate, a lid for covering the loading well and a second lid for covering the wells in the manifold body. The reversible seals described in Figure 3 of the paper served to consistently interface the manifold body with the 17 inlet/outlet holes of the microfluidic device. Figure S2.1A shows a photograph of the manifold body positioned with the bottom side up. The reversible seal connections to the artery chip distinguished with different colors are two fixation lines (blue color), one perfusion outlet (green color), one outlet for the bubble trap vacuum (turquoise color), one superfusion outlet (red color), six superfusion inlets (red color, 1, 2, 4, 5, 6, 8), six actuation lines (red color, I, II, III, IV, V, VI). Figure S2.1B shows a rendered schematic from a perspective similar to the one in Fig. S2.1A.

Figure S2.1C shows a photograph of the top side of the manifold body and the artery chip assembled to the manifold base plate. The lid covering the loading well as well as the separate lid covering the pressurized superfusion wells are not mounted in the image. Of the nine wells, wells 1, 2, 4, 5, 6, 8 are being used in this work and are fluidically connected to the chip via reversible seals as shown in Figs. 3B-F and Fig. S2.1A. The wells are subjected to the common superfusion head pressure p_A . Six miniature solenoid valves are labelled I-VI, (model LHLA0521111H, Lee Company, Westbrook, CT, USA) in Figs. S2.1C and S2.1D and used to actuate corresponding membrane valves on the artery chip. The compact manifold body minimizes dead volumes, removes the need for using external pumps, is robust and easy to use.

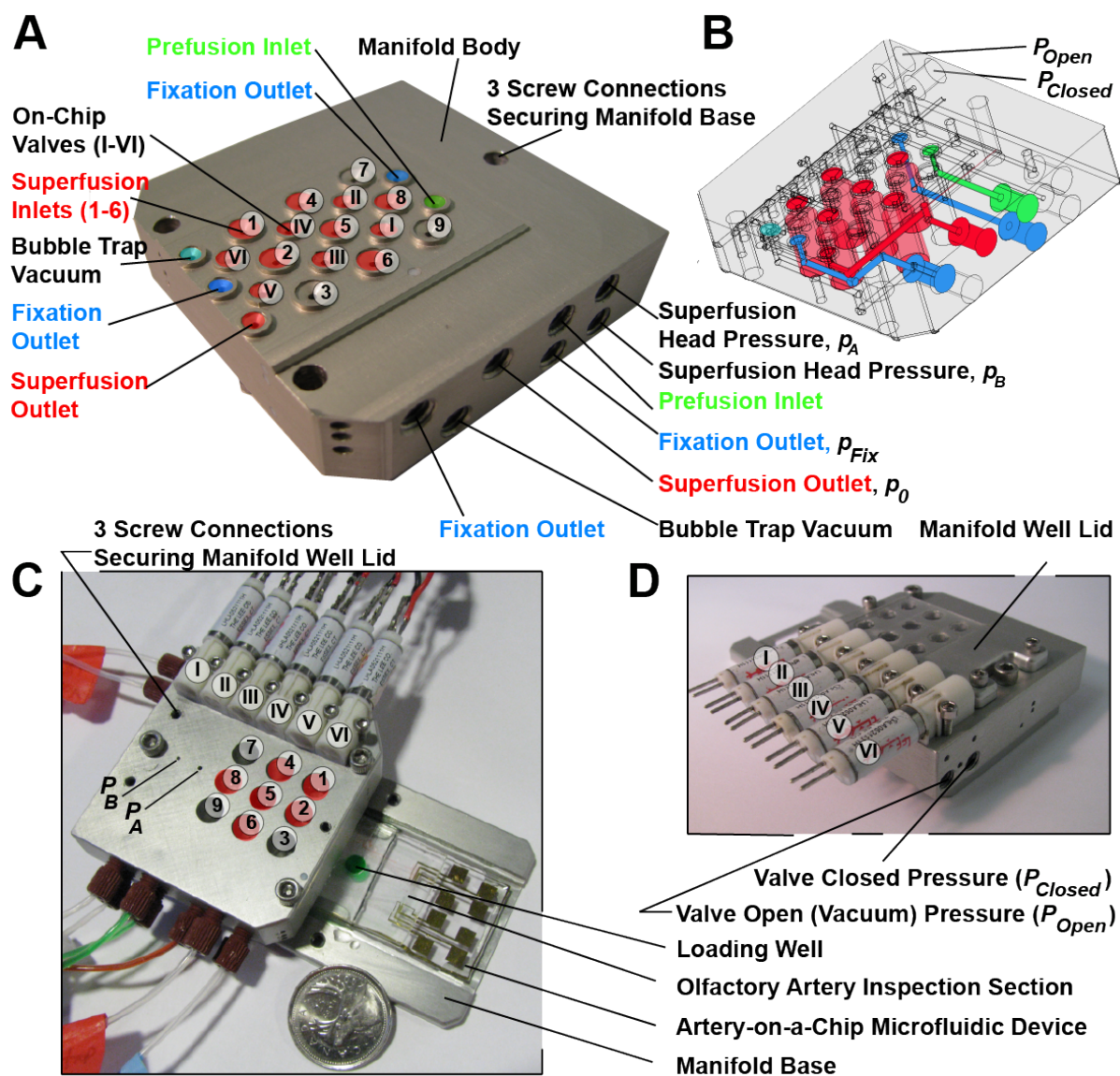


Figure S2.1 (A) Photograph (bottom view) of manifold body with 17 employed reversible fluidic connections between manifold and microfluidic artery-on-a-chip device (see Fig. S1.1) highlighted in by color (red: superfusion, green: perfusion, blue: fixation, in total 19 reversible fluidic connections available). (B) Perspective view of 3D manifold design (selected perspective similar to one shown in panel A) with color-coded internal fluidic connections. (C) Photograph (top view) of manifold body and artery-on-a-chip microfluidic device assembled to manifold base. Loading well open, i.e., manifold well lid not attached. Six wells shown in red color (i.e., “1”, “2”, “4”, “5”, “6”, and “8”) store superfusion solutions. Miniature solenoid valves (I-VI) directly attached to manifold body for actuation of individual on chip valves. Canadian Quarter coin shown for comparison. (D) Photograph of manifold well lid assembled to manifold body (manifold base and artery-on-a-chip device not attached).

We incorporated liquid fillable wells within a compact manifold design as opposed to the microfluidic device, in order to make best use of the available device footprint without significantly increasing dead volumes. Short response times of ~ 1 s were achieved by controlling superfusion flow via microfabricated membrane valves. All actuation lines for on-chip valves were initially primed with water by submerging the device in an open vial of deionized water at vacuum (-20 inHg) overnight. The approach consistently prevented unwanted bubble formation in the superfusion lines during valve actuation.

Biological buffer solutions, vasoactive substances, or staining reagents were preloaded into individual wells at volumes of approximately 350 μ l. The wells can be conveniently refilled during the course of one experiment by temporarily reducing the head pressure to atmospheric pressure, and then removing the well cover. Refilling was only necessary during dose-response experiments (Table S6.3) because the number of solutions required exceeded the number of available wells (i.e., not because a well emptied and needed to be refilled). At a typical flow rate of 0.5 μ l/min one well filling allowed maintaining a constant superfusion flow during more than 10 hours. Outflow from a particular well into the superfusion channel was enabled by activating an on-chip valve².

S3. On-Chip Valves

The on-chip valves were designed and fabricated as previously described by Irima *et al.* [4]. We used a simple microfluidic chip design with the microchannel footprint shown in Fig. S3.1A to characterize the on chip valves. The device accommodates two on-chip valves with individual actuation lines. The microchannels for each valve meet at a downstream mixing point prior to flowing out the outlet. The device was fabricated as described in Fig. S1.2.

Figure S3.1B provides a schematic of the experimental setup used for the characterization of the on-chip valves. The inlet and outlet ports of the device were connected to reservoirs positioned at fixed hydrostatic head levels.

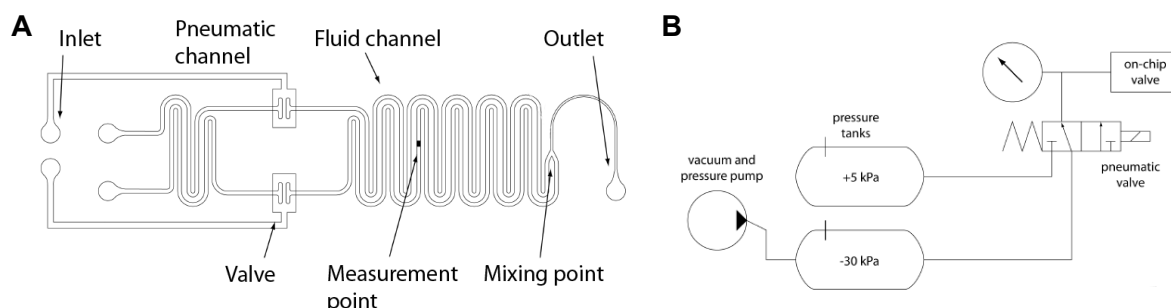


Figure S3.1 (A) Microchannel footprint of microfluidic device used for characterization of on-chip valves. (B) Schematic of experimental setup.

The response time of the valves was measured via particle image velocimetry (PIV). Water was seeded with $1\mu\text{m}$ Nile red fluorescent microspheres (Invitrogen, Carlsbad, CA, USA) that were illuminated with a green double-pulse laser (wavelength 532nm, model Nd:YAG Solo PIV, New Wave Research, Fremont, CA, USA) and imaged using an inverted fluorescence microscope and projected onto a double shutter digital camera (model Sensicam UV, PCO, Kelheim, Germany). Image pairs were acquired at a delay time of $\Delta t = 200\mu\text{s}$ and processed using a commercial PIV correlation engine (version DaVis 7.2, LaVision, Göttingen, Germany). Figure S3.2 shows the time-dependent spatial averages of the measured velocity vectors. The full time profile was obtained by using the solenoid valve signal as an external trigger for PIV image acquisition.

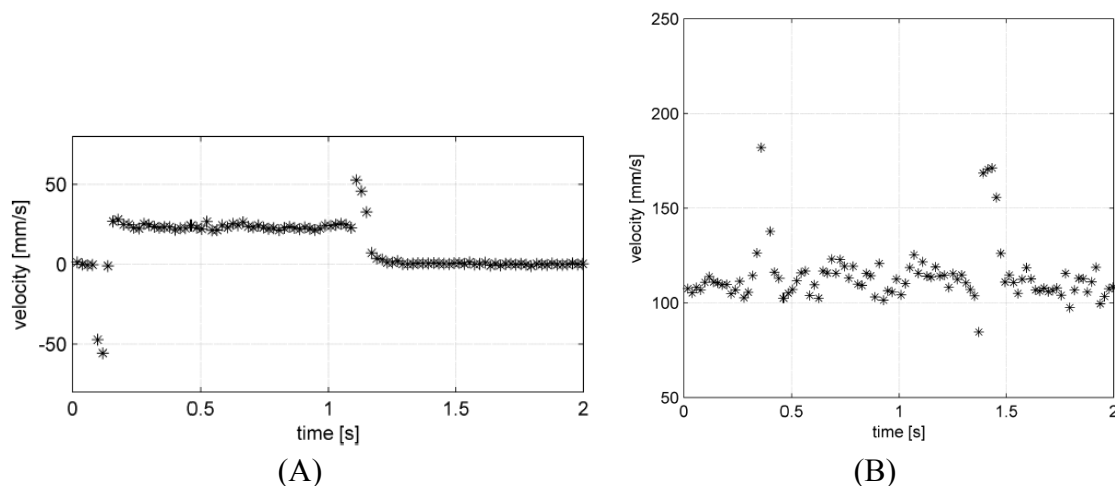


Figure S3.2 (A) Temporal variation of the spatially averaged measured fluid velocity during opening/closing of on-chip valve. Velocities were measured using microscale particle image velocimetry. (B) Representative plot of fluid velocity after “mixing point” while switching between two on-chip valves.

Based on our measurements we estimate the opening and closing time of the on-chip valves to be approximately 0.2 s. During the actuation of an on-chip valve the measured fluid velocity rapidly changes due to the sudden displacement of fluid beneath the PDMS membrane (Fig. S3.2A). When the valve opened, the membrane lifted up, drawing liquid towards the valve, corresponding to a temporarily negative fluid velocity. When the valve closed, the fluid was displaced in the direction away from the valve, resulting in a temporarily positive fluid velocity. The measured velocity minima and maxima were found to depend on the microchannel geometry as well as the fluid resistances upstream and downstream of an on-chip valve. In the context of our artery-on-a-chip devices, on-chip valves were employed to connect only one of the several fluid reservoirs on the manifold with the superfusion channel at any given point in time.

To further investigate the effect of the time changing fluid velocity associated with one on-chip valve closing and another one opening, the previously described experiment was repeated while taking measurements downstream of the location where two individually

addressable microchannels meet as shown in Fig. S3.1A. Figure S3.2B shows the time dependent velocity distribution. We observed an instantaneous peak velocity approximately equal to two times the nominal flow rate, and a peak duration of approximately 0.2ms. When we performed a similar experiment with artery-on-a-chip devices and chip hosted blood vessels switching between superfusion reservoirs did not noticeably affect the position of the arterial wall.

Finally, the need for applying a vacuum while opening the on-chip valve was tested under conditions relevant for our artery-on-a-chip microfluidic device. The removal of the vacuum would ease the operation of the valve by removing the necessity of a vacuum pump. The velocity was measured using PIV as described above. Image pairs were acquired at a rate of 5 frames per second and averages were calculated over an ensemble of 200 velocity vectors. The resultant plot is shown in Fig. S3.3.

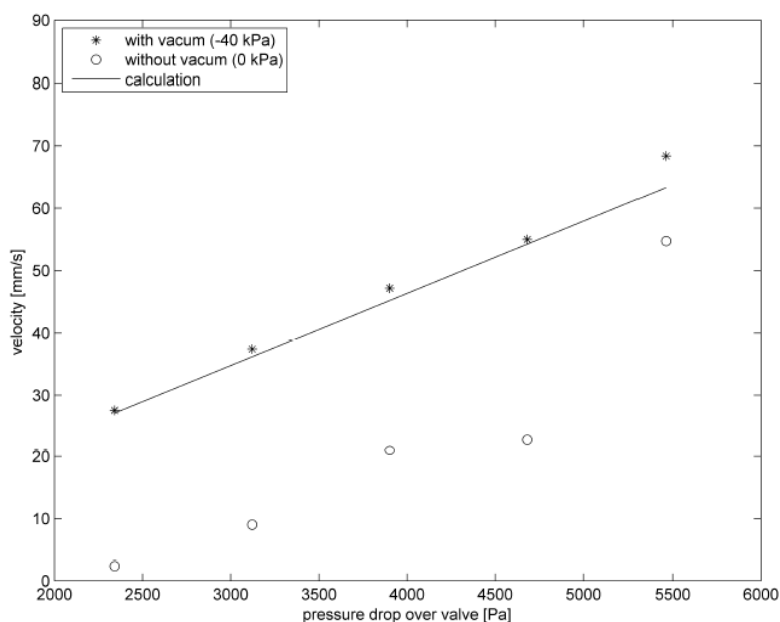


Figure S3.3 Effect of vacuum pressure on liquid velocity in microchannel caused by different degrees of opening of on-chip valve.

Figure S3.3 suggests that without the application of a vacuum a minimum pressure of 2000 Pa was required in the liquid channel upstream of the on-chip valve for opening the valve. The measured relationship between the liquid velocity and the pressure difference applied across the valve is non-linear. The finding is expected, as with increasing pressure the fluid pressure causes the valve to open. As a result, the available cross-section increases and reduces the resistance to flow.

However, if the valve was operated while applying a vacuum in its open state, the consistent operation of the on-chip valve could be extended to very small liquid velocities while the velocity maintained a desirable a linear trend, indicating a constant fluidic resistance. In the case of the artery-on-a-chip microfluidic device, vacuum was therefore applied when keeping the on-chip valves in their open state and allowed for consistent operation at low superfusion pressures (max 1000 Pa).

S4. On-Chip Temperature Control

We previously described our approach of establishing a uniform temperature field over the inspection area of artery-on-a-chip elastomeric devices while providing optical access for transmission imaging.³ A similar approach was applied here. Physiological temperature was established at the inspection section of the microfluidic device via a single mode temperature controller (model TE-48-20, TE Technology, Traverse City, MI, USA) that was electrically connected to a thermoelectric (TE) element (model TE-35-0.6-1.0, TE Technology). The latter provided for either heating or cooling in feedback control with a thermistor (model MP-2444, TE Technology) that was attached via thermally conductive epoxy (thermal conductivity $7.9 \text{ Wm}^{-1}\text{K}^{-1}$) to a sapphire disk (diameter: 25mm, thickness: 1mm, thermal conductivity: $35 \text{ Wm}^{-1}\text{K}^{-1}$, model WSR-251, UQG Optics, Cambridge, UK) to uniformly

spread heat across the inspection area. The selected configuration provided a constant temperature distribution in the horizontal direction where the sapphire disk was in contact with the PDMS. However as heat was conducted through an approximately 3 mm thick layer of PDMS (thermal conductivity: $0.1 \text{ Wm}^{-1}\text{K}^{-1}$), the temperature at the artery location differed from the one at the sapphire disk. To accurately establish physiological temperature at the location of the artery segment, temperature measurements were obtained using the thin-film resistance thermometers that were patterned on the superfusion inflow and outflow sides of the inspection area (see Fig. 2G, Fig. S2.1C). Two resistance thermometers were patterned to provide redundancy. Thin film resistors were lithographically patterned onto a glass slide that was covered with a 10 nm adhesion layer of titanium and a 100 nm thick layer of gold (Fig. S4.1A). The patterned electrode patterns showed an electrical resistance that linearly varied with temperature and was therefore suitable for measuring the artery temperature. Measurements were conducted using a four point sensing configuration, i.e., current lines leading to the electrode were separated from voltage sensing across the region to be measured. A constant current of 5mA was provided by the circuit shown in Fig. S4.1B. For calibration, each assembled microfluidic device was capped with a glass slide containing thin film resistors was submerged within a 30ml Eppendorf tube, placed in a circulating water bath (SC100-A10, Thermo Scientific, USA) along with a reference resistance thermometer. During calibration, each temperature set point was applied for 10 min, prior to taking a voltage reading on the reference thermometer. Figure S4.1C shows a representative calibration plot for one device and represents a linear relationship between the voltage, V and the temperature, $T = aV + b$, with the coefficients $a = 0.72 \text{ mV}^{-1}$, $b = -383^\circ\text{C}$.

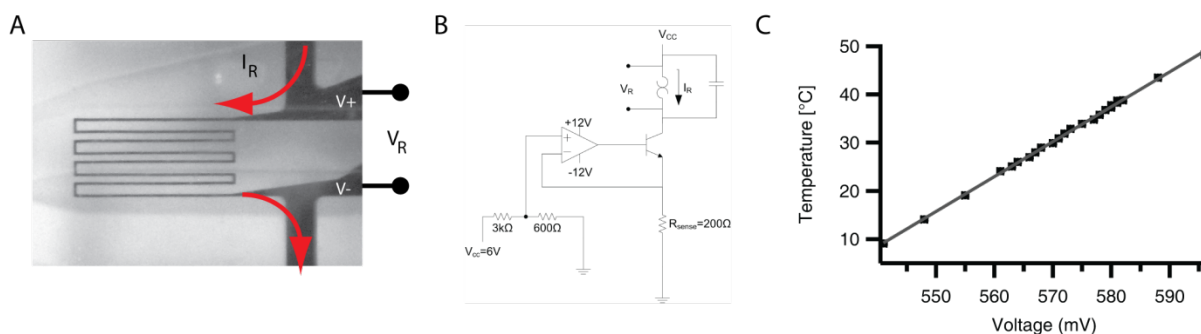


Figure S4.1 (A) Enlarged view of thin film electrode pattern with current flow and voltage measurement branches. (B) Schematic circuit diagram for 5mA current source used to power on-chip temperature sensitive electrode. Voltage drop measured using National Instruments data acquisition board. (C) Representative calibration curve obtained with constant 5mA supply current.

The thin-film sensor based temperature readings were used to incrementally adjust the set point of the thermoelectric controller via a proportional gain software controller (see Fig. S4.2) and imposed the physiological target temperature (37.0 ± 0.5 $^{\circ}C$) at the location of the artery. Temperature control, valve actuation and the interface with digital pressure regulators were programmed in a custom software program (LabView, National Instruments, Austin, TX, USA) and addressed using a data acquisition board (model DAQ6008, National Instruments). The software program allowed either manual operation via a user interface, or automated control according to a pre-set input. In the latter case, a text file describing the time sequence of events was read in a master timing loop that supplied each individual sub-loop with the necessary states: the valve state, the temperature set points and the pressure set point (see Section S6 for the LabView programs and Section S7 for the programmed staining sequences). For cooling the artery segment as required by some of the staining protocols, a simple circuit was prepared that interfaced with the software program to switch the polarity on the TE controller, and a large heat sink and fan were attached to the TE controller for heat

removal. Alternatively, to avoid the use of a heat sink and fan, the manifold and loaded artery chip was placed in ice to rapidly cool the chip.

A proportional-integral-derivative controller (PID controller, TE Technologies, Traverse City, MI, USA) was used to operate the thermoelectric element in feedback control from a temperature measurement obtained from a thermistor that was attached to the sapphire disk. The temperature difference between the thermistor and the thin-film recording was then used to adjust the set point of the controller as indicated in Fig. S4.2A. The configuration provided a proportional gain controller with gain value of 1. Figure S4.2B shows the temperature response to an imposed step change increase (solid blue line) as recorded on-chip using the patterned thin film resistance thermometer (solid red line) in comparison with the readout from the sapphire-mounted thermistor (dotted red line). The temperature measured by the thermistor followed the set point and the temperature at the location of the blood vessel was significantly lower. Figure S4.2C shows the heating protocol using for the implemented control system where the set point was applied to the temperature of the blood vessel as measured by the thin film RTD in accordance with the control system shown in Fig. S4.2A. The dotted blue line indicates the set point sent to TE controller (SP_{TE}), while the solid blue line is the actual set point. The calibrated thin film resistors and PID controller allowed to consistently maintain the chip-hosted artery at either 37.0°C, or at 4.0°C, as required during the dose-response or staining protocols.

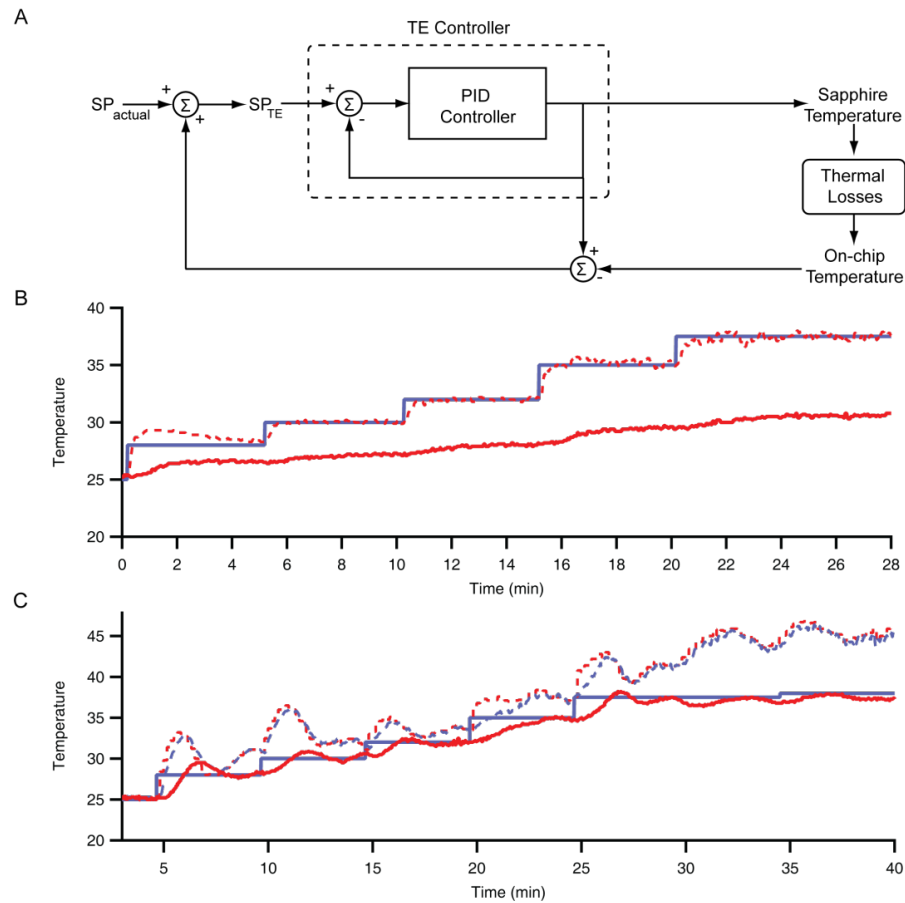


Figure S4.2 (A) Control system for maintaining artery at desired temperature. (B) Response to step change increase in temperature following heating protocol for artery segments, showing clear offset between temperature readings of on-chip RTD and sapphire-mounted thermistor. Solid blue line indicates temperature set point, solid red line is on-chip temperature measured by RTD, and dotted red line is temperature of sapphire disk. (C) Heating protocol using modified control system. On-chip temperature reaches required set point. Dotted blue line indicates set point sent to TE controller (SP_{TE}). Solid blue line is actual set point.

S5. Numerical Model for Abluminal Shear Stress Distribution

A numerical simulation of the superfusing flow around the chip-hosted artery segment was conducted using the multiphysics program Comsol (version 4.2, Comsol, Burlington, MA, USA). The computational domain and the boundary conditions are indicated in Fig. S5.1. The flow field is only solved for the domain highlighted in dark blue. The boundary

condition at the inlet was a parabolic velocity profile with a total flow rate of $0.25\mu\text{l}/\text{min}$ that corresponded to a total superfusion flow rate of $0.5\mu\text{l}/\text{min}$. A (gage) pressure of 0 Pa was applied at the outlet.

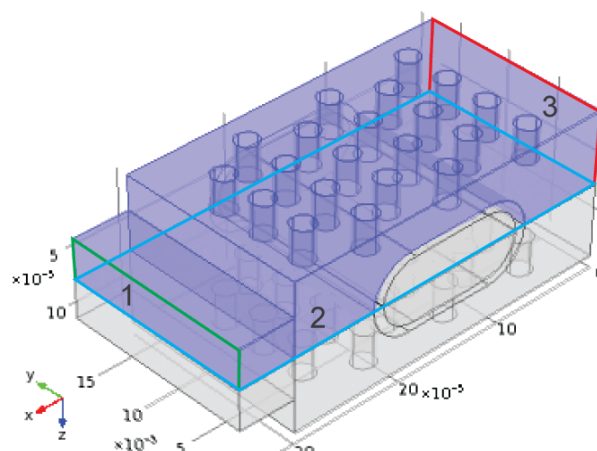


Figure S5.1 Computational domain for simulation of flow over chip-hosted artery segment containing pillar array. (1) Superfusion inflow into computational domain (outlined in green color), (2) microchannel center at which symmetry boundary condition was applied (outlined in turquoise color), (3) superfusion outflow region (outlined in red color). No slip boundary condition applied at all microchannel walls and outer blood vessel wall.

Table S5 summarizes results from a mesh independence study that were performed with two mesh sizes. Mesh 2 consisted of 4.8 times more elements as compared to Mesh 1. The largest difference in the results obtained for the two meshes was in the peak shear stress, varying by 0.5%. Based on the results summarized in Table S5 we considered the mesh resolution in our numerical simulation to be sufficiently high.

Table S5 Assessment of mesh independence for numerical simulation.

Compared Properties	Mesh 1	Mesh 2	Percentage Difference
Mesh elements	231,386	1,113,752	48.12%
Average wall shear rate across abluminal wall of	204.60 s^{-1}	204.64 s^{-1}	0.02%

artery			
Peak shear stress	573.61	570.68	0.5%
Volumetric flow rate at outflow section	4.16667× 10 ⁻¹² m ³ /s	4.16667× 10 ⁻¹² m ³ /s	<0.01%

S6. Automation

Table S6 displays a sample text file prepared for the automated small artery heating and administering a “wake up dose” of the vasoconstrictor PE. The custom Labview code shown in Fig. S6.1 reads each row of the text file and parses the columns to the appropriate actions. The first column contains the time spent at each step. The second column is the decimal representation of an 8-bit binary number, with each bit controlling the on/off state of a specific well (bits 7 and 8 are ignored since we only require the concurrent control of 6 wells in the presented study).

In the manual operating mode, the corresponding LabView code, shown Fig. S6.2, automatically detects when a change is made and closes the previously open well to minimize unwanted fluid feedback and pressure fluctuations between wells when actuated. To accommodate this in automatic mode, the binary representation of the well to be open must also account for this. Between states where a change is occurring, the common bit is the well that closes, and the different bit opens (an XOR operation). For example, in Table S6, between rows 5 and 6, well 1 closes, and well 4 opens. Between rows 6 and 7, the wells switch back from well 4 to well 1 (since just before the switch, the state of the wells is [0001000]). A row that is the same as the current state (row 8) results in no change. The third column is the temperature set point. The final two columns are pressure set points for the pressure heads controlling the external perfusion reservoir, and the superfusion wells.

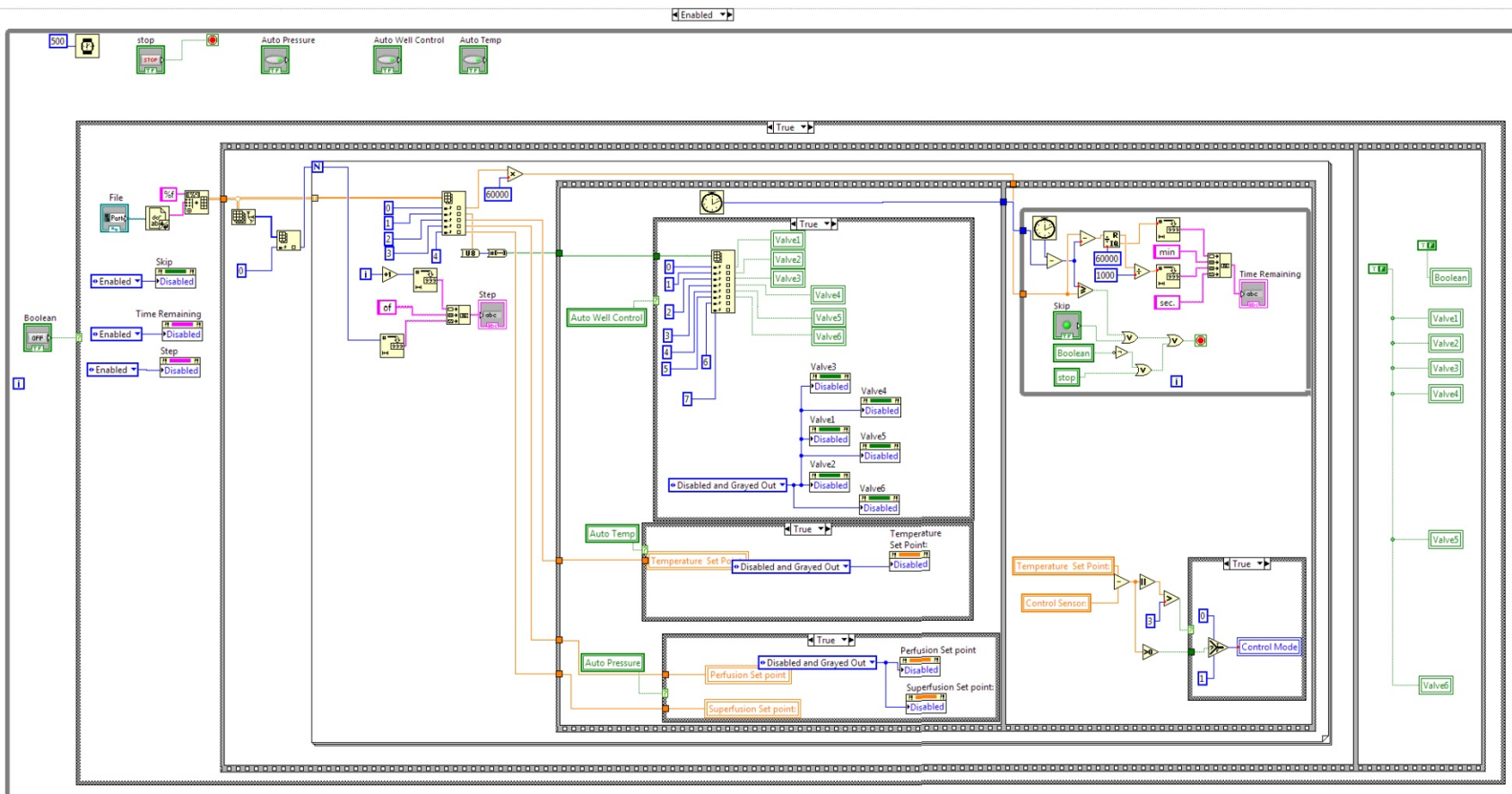


Figure S6.1 Graphical representation of Labview code responsible for parsing text file input for automated control of on-chip valves, artery segment temperature, and pressure regulators.

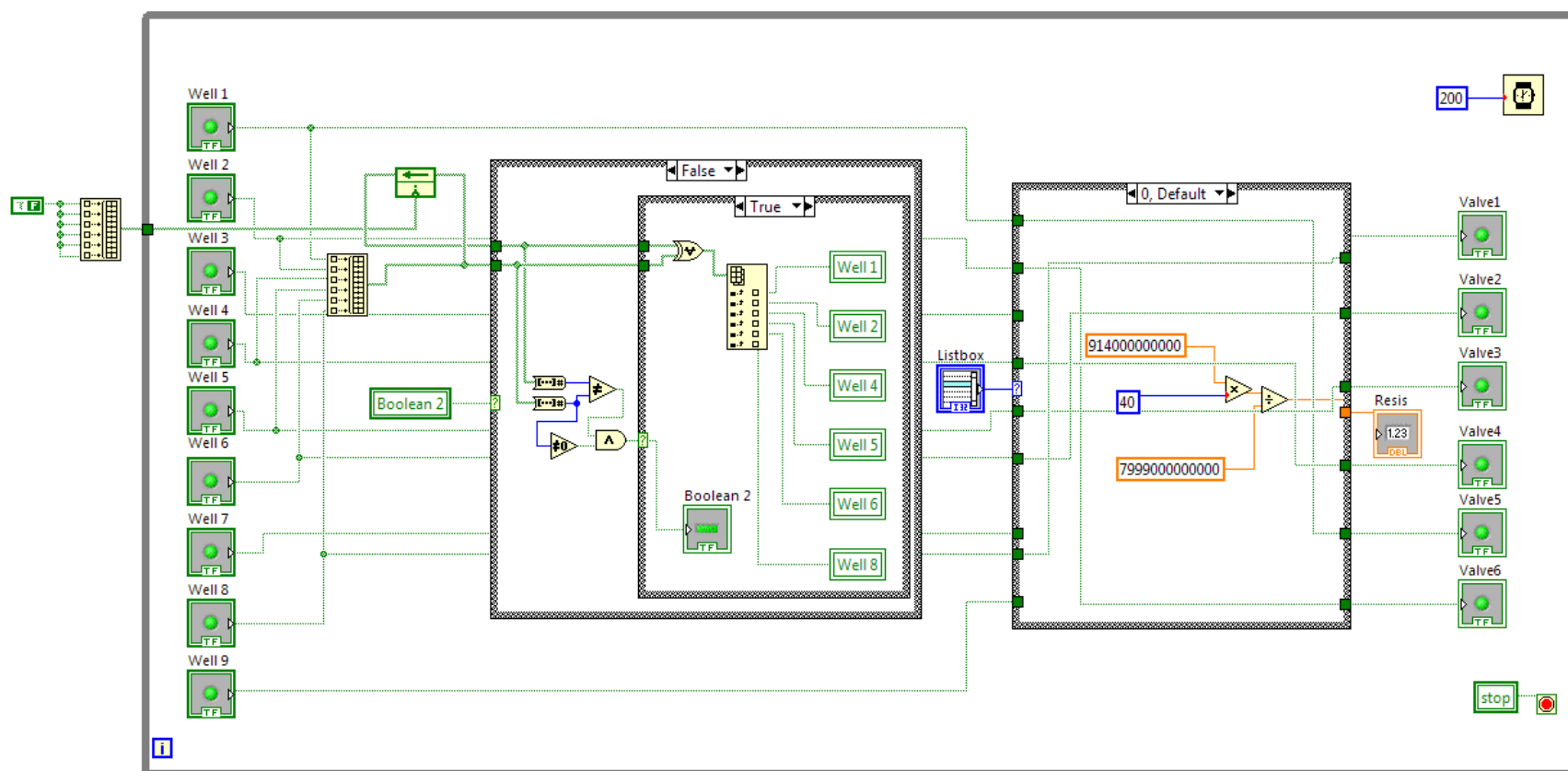


Figure S6.2 Graphical representation of LabView code responsible for actuating valves based on commands for opening six fluid wells on manifold for dose response and staining experiments. Listbox allows configuring well-to-valve connections for various chip designs. The code also allows estimating fluidic resistance in order to predict flow rates based on applied superfusion inlet pressures.

Table S6. Example of tab delimited text file used to absolve automated sequences. The binary representation of settings in column two, indicated in square brackets, is shown for explanatory purpose only, typical text files include only the decimal value.

Time (min)	Active Well, States of Valves [I-II- III-IV-V-VI]	Temperature (°C)	Perfusion Pressure (mmHg)	Superfusion Pressure (mmHg)
15	1 [00000001]	25	45	5
10	1 [00000001]	28	45	5
10	1 [00000001]	31	45	5
10	1 [00000001]	34	45	5
20	1 [00000001]	37.5	45	5
1	9 [00001001]	37.5	45	5
1	9 [00001001]	37.5	45	5
10	1 [00000001]	37.5	45	5

S7. Automated Dose Response and Staining Experiments

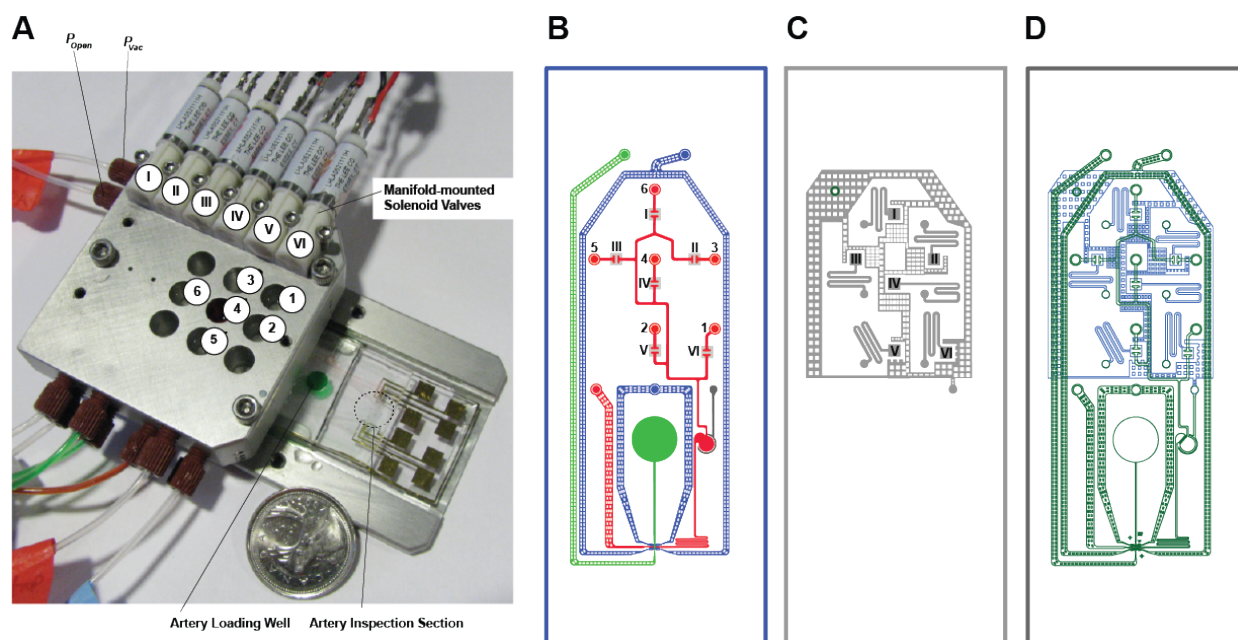


Figure S7.1 (A) Manifold containing wells and solenoid valves used in protocols with valve and well labels corresponding to their corresponding inlets in figure panels (B) and (C). Canadian quarter coin (diameter 23.8 mm) shown for comparison. (B) Buffer-perfused layer of artery-on-a-chip device (i.e., bottom layer) with corresponding locations of co-axially aligned superfusion wells labeled. Chip-hosted artery resides in this layer. (C) Actuation layer of artery-on-a-chip device (i.e., top layer) with inlets corresponding to control valves labeled in panel (A). (D) Microchannel footprint of artery-on-a-chip device with both buffer-perfused bottom layer and top actuation layer.

Table S7.1 Protocol used for cytoskeletal staining.

Step	Solution	Time (min)	Temp (°C)	Superfusion Pressure (mmHg)	Perfusion Pressure (mmHg)
Cytoskeleton Stains	Buffer (1,[000001])	10	37.5	5	45
	Buffer	2	4	5	45
	4% PFA (6,[100000])	30	4	5	45
	0.5% Triton X (5, [001000])	30	4	5	45
	1% BSA (4, [000100])	30	25	5	45
	Alexafluor 594 Phalloidin DAPI (2, [000010])	120	25	5	45
	Buffer (1,[000001])	10	25	10	45

Total duration of automated staining sequence

262 min (4.37 hrs)

Figure S7.1A shows the six manifold wells (labelled “1” to “6”) that were used to perform automated staining experiments along with the corresponding solenoid valves (labelled “I” to “VI”) that initiated outflow into the superfusion channel. Figure S7.1B shows the liquid perfused bottom layer of the artery-on-a-chip microfluidic device. Figure S7.1C shows the top actuation layer.

Automated co-staining of a chip-hosted artery segment was performed with Phalloidin (F-actin) and DAPI (nuclei). No remodeling was observed in proximity of pillar-supported areas of the vascular wall during the relatively short duration of our on-chip functional assessment (i.e., less than 4 hours). Remodelling during longer experimental times was not investigated. Imaging confirmed the expected exclusion of actin from smooth muscle cell nuclei. Nuclear eccentricity was evaluated using the relationship

$$e = \sqrt{1 - \left(\frac{\text{minor axis length}}{\text{major axis length}} \right)^2}.$$

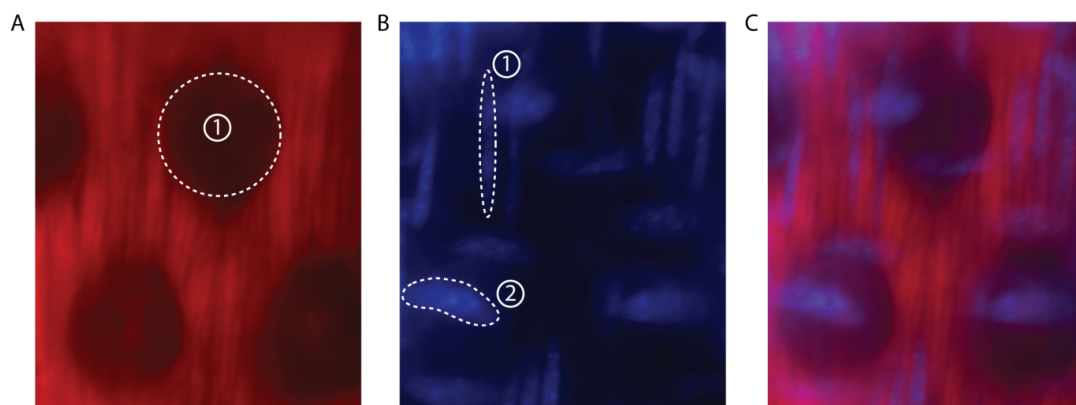


Figure S7.2 Enlarged view of wide-field fluorescence micrograph of co-stained cerebral artery segment obtained at 10× magnification with blood vessel axis aligned horizontally. (A) Actin staining, where region (1) corresponds to pillar location. (B) Nuclear staining of same region as shown in panel (A). Region (1) corresponds to nuclear stain of SMC and region (2) corresponds to EC nuclei. (C) Overlay of actin and nuclear channels indicated expected exclusion of phalloidin stain from nuclei.

Immunofluorescence. Negative control for L-type calcium channel was conducted by pre-incubating with peptide antigen corresponding to amino acid residues 848-865 of rat $Ca_v1.2$ provided with the antibody (Alomone Labs, Jerusalem, Israel) at equivalent concentration by weight (16 μ g/ml).

Table S7.2 Protocol used for Calcium channel immunostaining.

Step	Solution	Time (min)	Temp (degC)	Superfusion Pressure (mmHg)	Perfusion Pressure (mmHg)
Immunostain	Buffer (1,[000001])	10	37.5	5	45
	Buffer	2	4	5	45
	4% PFA (6,[100000])	30	4	5	45
	0.5% Triton X (5, [001000])	30	4	5	45
	1% BSA (3, [010000])	30	4	5	45
	1:50 Anti $Ca_v1.2$ (2, [000010])	600	4	2	45
	Buffer (1,[000001])	5	25	10	45
	1:1000 Alexafluor Anti rabbit Igg (4,[000001])	120	25	5	45
	Buffer(1,[000001])	10	25	10	45
	Total duration of automated staining sequence		837 min (13.95 hrs)		

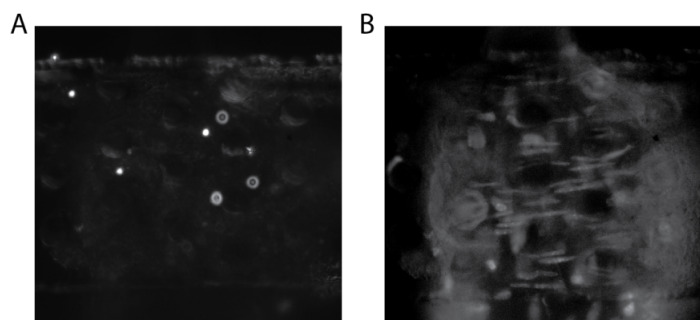


Figure S7.3 (A) Negative control for immunostaining. (B) Artery segment used for negative control, also DAPI stained.

Table S7.3- Protocol used for combined calcium imaging and dose response experiments. Valve state is assigned with a six-digit boolean number. Each digit corresponds to a single control valve as identified in Fig. S7.1A. A value of “1” indicates the valve “ON” state and “0” the “OFF” state.

Step	Solution (Active Well #, Valve States [I-II-III-IV-V-VI])	Time (min)	Temp (°C)	Superfusion Well Pressure (mmHg)	Perfusion Pressure (mmHg)
Load Artery	Buffer	-	25	-	-
Heating	Buffer (1,[000001])	5	25	5	45
	Buffer	5	28	5	45
	Buffer	5	31	5	45
	Buffer	5	35	5	45
	Buffer	10	37.5	5	45
Wake up	10uM PE (4,[000100])	1	37.5	10	45
	Buffer (1,[000001])	10	37.5	5	45
Dose Response	Buffer (1,[000001])	1	37.5	10	45
	0.1uM PE (3,[010000])	1	37.5	10	45
	1uM PE (6,[100000])	1	37.5	10	45
	5uM PE (5,[001000])	1	37.5	10	45
	10uM PE (4,[000100])	1	37.5	10	45
	Buffer (1,[000001])	1	37.5	10	45
	Buffer	10	37.5	5	45
Remove lid and add dye to well 2					
Calcium Stain	2uM FURA2-AM (2,[000010])	90	37.5	5	45
	Buffer (1,[000001])	10	37.5	5	45
Dose Response	Buffer (1,[000001])	1	37.5	10	45
	0.1uM PE (3,[010000])	1	37.5	10	45
	1uM PE (6,[100000])	1	37.5	10	45
	5uM PE (5,[001000])	1	37.5	10	45
	10uM PE (4,[000100])	1	37.5	10	45
	Buffer (1,[000001])	1	37.5	10	45
	Buffer	10	37.5	5	45
Remove lid, rinse all dye out of well 2 and load Nifedipine into well 2					
Calcium Blocker	1uM Nifedipine (2,[000010])	30	37.5	5	45
	Buffer (1,[000001])	10	37.5	5	45
Dose Response	Buffer (1,[000001])	1	37.5	10	45
	0.1uM PE (3,[010000])	1	37.5	10	45
	1uM PE (6,[100000])	1	37.5	10	45
	5uM PE (5,[001000])	1	37.5	10	45
	10uM PE (4,[000100])	1	37.5	10	45
	Buffer (1,[000001])	1	37.5	10	45
	Buffer	10	37.5	5	45

Total duration of automated staining sequence 231 min (3.85 hrs)

Supplementary References

1. M. A. Eddings, M. A. Johnson and B. K. Gale, *J. Micromech. Microeng.*, 2008, **18**, 4.
2. C. Lochovsky, S. Yasotharan and A. Gunther, *Lab Chip*, 2012, **12**, 595-601.
3. A. Gunther, S. Yasotharan, A. Vagaon, C. Lochovsky, S. Pinto, J. Yang, C. Lau, J. Voigtlaender-Bolz and S.-S. Bolz, *Lab Chip*, 2010, **10**, 2341-2349.
4. D. Irimia, M. Toner, *Lab Chip*, 2006, **3**, 345-352.